Critical transition in fast-rotating turbulence within highly elongated domains

Adrian van Kan[1]†, and Alexandros Alexakis [1]

[1]Laboratoire de Physique de l'Ecole normale supérieure, ENS, Université PSL, CNRS, Sorbonne Université, Université Paris-Diderot, Sorbonne Paris Cité, Paris, France

(Received xx; revised xx; accepted xx)

We study rapidly-rotating turbulent flows in a highly elongated domain using an asymptotic expansion at simultaneously large rotation rate $\Omega = O(1/\epsilon)$ and domain height $H = O(1/\epsilon)$, $\epsilon \ll 1$. We solve the resulting equations using an extensive set of direct numerical simulations for different parameter regimes. As a parameter $\lambda \propto \Omega/H$ is increased beyond a threshold λ_c, a transition is observed from a state without an inverse energy cascade to a state with an inverse energy cascade. For large Reynolds number and large horizontal box size, we provide evidence for criticality of the transition in terms of the large-scale energy dissipation rate and estimate a critical exponent close to unity.

Key words:

1. Introduction

Rotating fluid flows are commonly encountered in astrophysical and geophysical systems such as planetary and stellar interiors, planetary atmospheres and oceans (Pedlosky 2013), as well as in industrial processes involving rotating machinery. The fluid motions in these systems are typically turbulent, i.e. the Reynolds number Re, which is defined as the ratio between inertial and viscous forces, is large. At the same time the flow is affected by the Coriolis force due to system rotation. The magnitude of the Coriolis acceleration compared to the inertial acceleration is measured by the non-dimensional Rossby number $\mathrm{Ro} = U/(\Omega\ell)$, where Ω is the rotation rate and U and ℓ are typical velocity and length scales of the flow. For $\mathrm{Ro} < \infty$, the isotropy of classical three-dimensional (3-D) turbulence is broken, since the rotation axis imposes a direction in space. When the rotation rate is large, i.e. in the limit $\mathrm{Ro} \to 0$, the rotation tends to suppress variations of the motion along the axis of rotation and thus makes the flow quasi-two-dimensional, an effect described by the Taylor-Proudman theorem (Hough 1897; Proudman 1916; Taylor 1917; Greenspan *et al.* 1968).

As is well known, the properties of turbulent cascades strongly depend on the dimension of space. In homogeneous isotropic 3-D turbulence, energy injected at large scales is transferred, by non-linear interactions, to small scales in a *direct energy cascade* (Frisch 1995). In the two-dimensional (2-D) Navier-Stokes equations both energy and enstrophy are inviscid invariants and this fact constrains the energy transfer to be from small to large scales in an *inverse energy cascade* (Boffetta & Ecke 2012). When Ro is lowered below a certain threshold value Ro_c in a rotating turbulent flow, a transition is encountered where the flow becomes quasi-2-D and an inverse cascade develops. In this state, part of

† Email address for correspondence: adrian.van.kan@phys.ens.fr

the injected energy cascades to larger scales and another part to smaller scales, forming what is referred to as a *split* or *bidirectional* cascade (Alexakis & Biferale 2018). In the absence of effective large-scale damping, this inverse cascade can lead to the formation of a condensate in which the energy is concentrated at the largest scale.

The formation of large-scale quasi-2-D structures in rotating flows has been observed early on in experiments (Ibbetson & Tritton 1975; Hopfinger *et al.* 1982; Dickinson & Long 1983) and numerical simulations (Bartello *et al.* 1994; Yeung & Zhou 1998; Godeferd & Lollini 1999; Smith & Waleffe 1999). Since then, various investigations have focused on different aspects of the quasi-2-D behaviour of rotating turbulence experimentally (Baroud *et al.* 2002, 2003; Morize & Moisy 2006; Staplehurst *et al.* 2008; Van Bokhoven *et al.* 2009; Duran-Matute *et al.* 2013; Yarom *et al.* 2013; Machicoane *et al.* 2016) and numerically (Mininni *et al.* 2009; Thiele & Müller 2009; Favier *et al.* 2010; Mininni & Pouquet 2010; Sen *et al.* 2012; Marino *et al.* 2013; Biferale *et al.* 2016; Valente & Dallas 2017; Buzzicotti *et al.* 2018*a*,*b*). In particular, recent experiments were able to investigate the presence of the inverse cascade (Yarom & Sharon 2014; Campagne *et al.* 2014, 2015, 2016). The transition from forward-cascading to inverse-cascading rotating turbulence was studied systematically using numerical simulations in (Smith *et al.* 1996; Deusebio *et al.* 2014; Pestana & Hickel 2019), while the transition to a condensate regime was studied in (Alexakis 2015; Yokoyama & Takaoka 2017; Seshasayanan & Alexakis 2018).

Similar transitions from a forward to an inverse cascade and to quasi-2-D motion have also been observed in other systems like thin-layer turbulence (Celani *et al.* 2010; Benavides & Alexakis 2017; Musacchio & Boffetta 2017; van Kan & Alexakis 2019; Musacchio & Boffetta 2019; van Kan *et al.* 2019), stratified turbulence (Sozza *et al.* 2015), rotating and stratified flows (Marino *et al.* 2015), magneto-hydrodynamic systems (Alexakis 2011; Seshasayanan *et al.* 2014; Seshasayanan & Alexakis 2016) and helically constrained flows (Sahoo & Biferale 2015; Sahoo *et al.* 2017) among others (see the articles by Alexakis & Biferale (2018) and Pouquet *et al.* (2019) for recent reviews).

While the existence of a transition from forward to inverse energy cascade is well-established in many systems, including rotating turbulence, its detailed properties remain poorly understood in most cases. Turbulent flows involve non-vanishing energy fluxes and thus are out-of-equilibrium phenomena (Goldenfeld & Shih 2017). While in the case of the laminar-turbulence transition in shear flows a connection with non-equilibrium statistical physics has been established by placing the problem in the directed percolation universality class (Pomeau 1986; Manneville 2009), in particular for plane Couette flow (Lemoult *et al.* 2016; Chantry *et al.* 2017) and pipe flow (Moxey & Barkley 2010), such a general theoretical link has yet to be found for the non-equilibrium transition from forward to inverse energy cascade. However, previous numerical studies have successfully analysed special cases. For instance in the case of thin-layer turbulence, Benavides & Alexakis (2017) were able to provide strong evidence for criticality of the inverse energy transfer rate as a function of a control parameter related to box height at the transition to an inverse cascade. The term criticality is used here to describe situations where an order parameter (e.g. the rate of inverse energy transfer) changes from zero to non-zero at a critical value of a control parameter (e.g. box height, Ro). When the limit of infinite horizontal box size and $Re \to \infty$ is taken this change can be either discontinuous (1st order) or continuous with discontinuous (first/second/higher) derivative (2nd order) at the critical point, (for a more detailed discussion, see (Alexakis & Biferale 2018)). Knowing whether the transition to an inverse cascade in a turbulent flow is critical or smooth is important, in particular since this information is paramount for further investigations. For instance, in a critical transition, two separated phases exist and one may meaningfully speak of the phase diagram of the system. This is particularly

interesting in situations with many parameters, such as rotating stratified turbulence in finite domains. Furthermore, near the critical points there are critical exponents to be measured, for which a comparison with theoretical predictions seems possible.

In the case of rotating turbulence in a layer of thickness H (after the limit of infinite horizontal box size L and Re is taken) there are two control parameters left as a function of which the system can display criticality: the ratio $h = H/\ell_{in}$ (where here ℓ_{in} is taken to be the forcing length scale) and Ro. If criticality is present, then this 2-D space (h, Ro) will be split into two regions, in one of which an inverse cascade is observed, but no inverse cascade in the other. The two regions are separated by a critical line given by $h_c(Ro)$ that needs to be determined. For large Ro (weak rotation), the problem reduces to that of the non-rotating layer and therefore $\lim_{Ro\to\infty} h_c(Ro) = h_c^* > 0$, where h_c^* is the critical value of h for the non-rotating layer (Celani *et al.* 2010; Benavides & Alexakis 2017; van Kan & Alexakis 2019). For small Ro, the scaling of h_c with Ro is not known. Deusebio *et al.* (2014) investigated this problem and showed evidence for a continuous transition, with h_c increasing as Ro was decreased but could not reach small enough Ro to determine a scaling of h_c with Ro. In (Alexakis & Biferale 2018) it was argued that the scaling $h_c \propto 1/Ro$ should be followed, but so far no evidence numerical or experimental exists to suppurt or dismiss this conjecture. This is what we address in this work by studying the simultaneous limit of asymptotically small Ro and large domain height.

The remainder of this paper is structured as follows. In section 2 we discuss the theoretical background of this study, in section 3, we introduce the set-up of our numerical simulations and define the quantities to be measured. In section 4, we describe the results of the direct numerical solutions (DNS) we performed and finally in section 5, we draw our conclusions and discuss remaining open problems.

2. Theoretical Background

2.1. *Quasi-two-dimensionalisation and wave turbulence*

In this section we discuss the theoretical results underpinning the present study. A fundamental property of rotating flows is the fact that they support inertial wave motions, whose restoring force is the Coriolis force (Greenspan *et al.* 1968). Inertial waves have the peculiar anisotropic dispersion relation

$$\omega^{s_{\mathbf{k}}}(\mathbf{k}) = 2s_{\mathbf{k}}\Omega k_{\parallel}/k, \tag{2.1}$$

where $s_{\mathbf{k}} = \pm 1$, Ω is the rotation rate, $k_{\parallel}$ is the component of $\mathbf{k}$ along the rotation axis and $k = |\mathbf{k}|$. Similarly, we define $k_{\perp}$ as the magnitude of the component of $\mathbf{k}$ perpendicular to the rotation axis. In the remainder of this article, *parallel* and *perpendicular* will always refer to the rotation axis. Inertial waves in fast-rotating turbulence are important for understanding the direction of the energy cascade, as will be discussed below. The form of (2.1) shows that motions which are invariant along the axis of rotation, i.e. which are 2-D with three components (2D3C), have zero frequency and are thus unaffected by rotation. This allows decomposing the flow into two components, the 2D3D modes which are not directly affected by rotation, forming the *slow manifold*, and the remaining 3-D modes which are affected by the rotation, forming the *fast manifold* (Buzzicotti *et al.* 2018*b*). In the limit Ro $\to 0$, it can be shown that only resonant interactions remain present (Waleffe 1993; Chen *et al.* 2005). Resonant interactions are those interactions between wavenumber triads $(\mathbf{k}, \mathbf{p}, \mathbf{q})$ satisfying

$$\mathbf{k} + \mathbf{p} + \mathbf{q} = 0, \tag{2.2}$$

$$\omega^{s_{\mathbf{k}}}(\mathbf{k}) + \omega^{s_{\mathbf{p}}}(\mathbf{p}) + \omega^{s_{\mathbf{q}}}(\mathbf{q}) = 0, \tag{2.3}$$

where $\omega^{s_{\mathbf{k}}}(\mathbf{k}), \omega^{s_{\mathbf{p}}}(\mathbf{p})$ and $\omega^{s_{\mathbf{q}}}(\mathbf{q})$ are given by (2.1). When only resonant interactions are present in the system, it can further be shown that any triad including modes from both the fast and slow manifolds leads to zero net energy exchange between the two manifolds. Thus, with only resonant interactions, the slow and fast manifolds evolve independently from each other without exchanging energy, and there is inverse energy transfer in the perpendicular components of the slow manifold. This decoupling may lead to an inverse energy cascade for the quasi-2-D part of the flow. In fact, it can be proven that for finite Reynolds number $Re \equiv U\ell/\nu$ (where ν is viscosity, U is r.m.s. velocity and ℓ is a forcing length scale) and finite H, the flow will become exactly 2-D as $Ro \to 0$ (Gallet 2015).

On the other hand, in the limit of infinite domain height H, very small values of $k_\parallel$ are possible, such that quasi-resonant triads, for which (2.3) is only satisfied to $O(\mathrm{Ro})$, can transfer energy between the slow and fast manifolds. Thus the inverse energy transfer in the slow manifold may be suppressed by interaction with quasi-resonant 3-D modes. Asymptotically, for infinite domains and $k_\parallel/k_\perp \ll 1$, wave turbulence theory predicts a forward energy cascade and an associated anisotropic energy spectrum (Galtier 2003).

There are thus two mechanisms at play in the energy transport: the dynamics of the slow manifold transferring energy to the large scales and the 3-D interactions transferring energy to the small scales. Which of these two processes dominates depends on the two non-dimensional parameters, the Rossby number $\mathrm{Ro} = \epsilon_{in}^{1/3}/(\ell_{in}^{2/3}\Omega)$, based on the velocity scale $(\epsilon_{in}\ell_{in})^{1/3}$ and the length scale ℓ_{in}, and the ratio $h = H/\ell_{in}$. The main criterion is whether or not 2-D modes are isolated from 3-D modes due to fast rotation. The coupling of 2-D and 3-D motions will be strong enough to stop the inverse cascade if the fast modes closest to the slow manifold ($k_\parallel \sim H^{-1}$, $k_\perp \sim \ell_{in}^{-1}$) are 'slow' enough to interact with the 2-D slow manifold. This implies that their wave frequency $\omega = 2\Omega k_\parallel/k_\perp \sim 2\Omega\ell_{in}/H$ is of the same order as the non-linear inverse time scale $\tau_{nl}^{-1} \sim \epsilon_{in}^{1/3}\ell_{in}^{-2/3}$. This leads to the following prediction for the critical height H_c, where the transition takes place,

$$h_c = \frac{H_c}{\ell_{in}} \propto \Omega\epsilon_{in}^{-1/3}\ell_{in}^{2/3} = \mathrm{Ro}^{-1}. \tag{2.4}$$

Importantly, the predicted critical rotation rate and height are linearly proportional. The criterion (2.4) suggests that the non-dimensional control parameter of the transition in the limit of large h and small Ro is given by

$$\lambda = \frac{1}{h \times \mathrm{Ro}} = \frac{\ell_{in}^{5/3}\Omega}{\epsilon_{in}^{1/3}H}. \tag{2.5}$$

2.2. *Multiscale expansion*

In the present paper, we will explore the regime of simultaneously large h and small Ro. Brute-force simulations at very small Ro are costly since very small time steps are required to resolve the fast waves of interest. Rather, we exploit an asymptotic expansion first introduced in (Julien *et al.* 1998), which allows to test the prediction (2.4) and to investigate the properties of the transition to a split cascade. The expansion is based on the Navier-Stokes equation including the Coriolis force and proceeds in the simultaneous limit of $H = \hat{H}/\epsilon$ and $\Omega = \hat{\Omega}/\epsilon$ with $\hat{\Omega}, \hat{H} = O(1)$ and $\epsilon \to 0$ (such that $\lambda = const. = O(1)$ according to 2.5), keeping the horizontal extent L of the domain fixed at order one, as depicted in figure 1. Note that height and rotation rate are proportional to each other, as in (2.4). By changing the prefactors $\hat{H}, \hat{\Omega}$, we can place ourselves above or below the critical line predicted by (2.4). In the following we drop the hats for simplicity. The method of multiple scales or a heuristic derivation (see appendix A) can be used to

obtain a set of asymptotically reduced equations for the parallel components of velocity $u_\parallel$ and vorticity $\omega_\parallel$,

$$\partial_t u_\parallel + \mathbf{u}_\perp \cdot \nabla_\perp u_\parallel + 2\Omega \nabla_\parallel \nabla_\perp^{-2} \omega_\parallel = \nu \nabla_\perp^2 u_\parallel + f_\parallel, \tag{2.6}$$

$$\partial_t \omega_\parallel + \mathbf{u}_\perp \cdot \nabla_\perp \omega_\parallel - 2\Omega \nabla_\parallel u_\parallel = \nu \nabla_\perp^2 \omega_\parallel + f_\omega, \tag{2.7}$$

with time t, velocity $\mathbf{u}$ and rescaled rotation rate Ω. The gradients $\nabla_\parallel, \nabla_\perp$ stand, respectively, for the derivative with respect to a slow parallel coordinate $\nabla_\parallel = \hat{e}_\parallel \cdot \nabla$, and for the horizontal gradients $\nabla_\perp = \nabla - \hat{e}_\parallel \cdot \nabla$ where $\hat{e}_\parallel = \boldsymbol{\Omega}/\Omega$. The velocity $\mathbf{u}$ is written in terms of $u_\parallel = \hat{e}_\parallel \cdot \mathbf{u}$ and $\mathbf{u}_\perp = \mathbf{u} - \hat{e}_\parallel u_\parallel$. The perpendicular components $\mathbf{u}_\perp$ are divergence-free to leading order $\nabla_\perp \cdot \mathbf{u}_\perp = \mathbf{0}$, which permits us to write them in terms of a stream function $\mathbf{u}_\perp = \hat{e}_\parallel \times \nabla\psi$ where ψ is such that $\omega_\parallel = \nabla_\perp^2 \psi$ and $\omega_\parallel$ is the vertical vorticity. The forcing $\mathbf{f}$ is written in terms of $f_\parallel = \hat{e}_\parallel \cdot \mathbf{f}$ and $\mathbf{f}_\perp = \mathbf{f} - \hat{e}_\parallel f_\parallel$, moreover we define $f_\omega = (\nabla \times \mathbf{f}) \cdot \hat{e}_\parallel$. In the following, $\mathbf{f}$ is chosen to be stochastic and, for simplicity, two-dimensional (invariant along the parallel direction), thus directly forcing the slow manifold. Furthermore $\mathbf{f}$ is filtered in Fourier space so that it is confined within a ring of wavenumbers centered on $k_f \equiv 1/\ell_{in}$. It is delta correlated in time, leading to a fixed mean energy injection rate $\langle u_\parallel f_\parallel \rangle = \langle \mathbf{f}_\perp \cdot \mathbf{u}_\perp \rangle = \epsilon_{in}/2 \Rightarrow \langle \mathbf{f} \cdot \mathbf{u} \rangle = \epsilon_{in}$, where $\langle \cdot \rangle$ denotes an ensemble average over infinitely many realisations. A similar 2-D forcing has been widely used in previous studies on the transition toward an inverse cascade, such as (Smith *et al.* 1996; Celani *et al.* 2010; Deusebio *et al.* 2014). We use random initial conditions whose small energy is spread out over a range of wavenumbers. Variants of the asymptotic equations (2.6, 2.7) have been extensively used in the past, in particular for studying rotating turbulence (Nazarenko & Schekochihin 2011) and rapidly rotating convection (adding energy equation) (Sprague *et al.* 2006; Julien *et al.* 2012*b*,*a*; Rubio *et al.* 2014; Grooms *et al.* 2010), as well as dynamos driven by rapidly rotating convection (adding the energy and MHD induction equations) (Calkins *et al.* 2015).

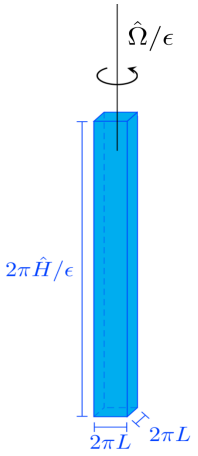

FIGURE 1. The long rapidly-rotating box domain.

The equations (2.6) and (2.7) are closely related to well-known models in geophysical fluid dynamics. In particular, since the leading-order horizontal velocity is in geostrophic balance, the model bears a resemblance to the classical quasi-geostrophic approximation. Indeed, equations (2.6, 2.7) have been referred to as *generalized quasi-geostrophic equations* (Julien *et al.* 2006).

A great advantage of the reduced equations over the Navier-Stokes equations is that while Ω and H are large in the original equation, they are of order one in the reduced equations, permitting much more efficient numerical integration. Importantly, equations (2.6) and (2.7) retain inertial waves with the correct dispersion relation, but only those with order-one frequencies. We perform direct numerical simulations (DNS) of (2.6) and (2.7) to show that, as predicted by the theory outlined above, there is indeed a transition from a direct to an inverse energy cascade in this extreme parameter regime.

3. Numerical set-up and methodology

In this section, we describe the numerical set-up used in the present study. We solve equations (2.6) and (2.7) numerically in a triply periodic domain of dimensions $2\pi L \times$

$2\pi L \times 2\pi H$ with modified dissipative terms. After nondimensionalising horizontal length scales based on ℓ_{in}, parallel length scales based on H and time based on the (eddy turnover) time scale $\tau_f = (\ell_{in}^2/\epsilon_{in})^{1/3}$ imposed by the forcing, we obtain the following PDEs to be solved,

$$D_t^{\perp} u_{\parallel} + 2\lambda \nabla_{\parallel} \nabla_{\perp}^{-2} \omega_{\perp} = -\frac{(-\nabla_{\perp}^2)^n u_{\parallel}}{Re_{\nu}} - \frac{(-\nabla_{\parallel}^2)^m u_{\parallel}}{Re_{\mu}} - \frac{u_{\parallel}^{ls}}{Re_{\alpha}} + f_{\parallel}, \tag{3.1}$$

$$D_t^{\perp} \omega_{\parallel} - \quad 2\lambda \nabla_{\parallel} u_{\parallel} \quad = -\frac{(-\nabla_{\perp}^2)^n \omega_{\parallel}}{Re_{\nu}} - \frac{(-\nabla_{\parallel}^2)^m \omega_{\parallel}}{Re_{\mu}} - \frac{\omega_{\parallel}^{ls}}{Re_{\alpha}} + f_{\omega}, \tag{3.2}$$

in the triply periodic domain of dimensions $2\pi\Lambda \times 2\pi\Lambda \times 2\pi$ with $\Lambda = L/\ell_{in}$. Note that the information about the parallel dimension is now contained in the parameter λ. Here $D_t^{\perp} = \partial_t + \mathbf{u}_{\perp} \cdot \nabla_{\perp}$. The right-hand side of eqs. (3.1,3.2) expresses the dissipation terms and the forcing. For a field g we define $g^{ls} = \sum_{\mathbf{k}, k_{\perp} \leqslant 2} \hat{g}(\mathbf{k}) \exp(i\mathbf{k} \cdot \mathbf{x})$, in terms of the Fourier transform $\hat{g}(\mathbf{k})$ of g with $\mathbf{k} \in \mathbb{N}^3$. The large-scale friction terms involving $u_{\parallel}^{ls}$ and $\omega_{\parallel}^{ls}$ have been added to prevent the formation of a condensate at small wave numbers. The term proportional to $\nabla_{\parallel}^{2m}(\cdot)$ suppresses exceedingly large parallel wave-numbers which are expected not to interact significantly with the slow manifold, thereby reducing the required resolution in the parallel direction and the computational cost. In all simulations $n = 4$ and $m = 2$ was used. The resulting equations (3.1,3.2) explicitly contain four non-dimensional parameters, in addition to Λ stemming from the boundary conditions. There are three different Reynolds numbers based on the three dissipation mechanisms $Re_{\nu} = \epsilon_{in}^{1/3} \ell^{2n-2/3}/\nu_n$, $Re_{\mu} = \epsilon_{in}^{1/3} \ell^{2m-2/3}/\mu_m$ and $Re_{\alpha} = \epsilon_{in}^{1/3}/(\ell^{2/3}\alpha)$, where ν_n is the hyperviscosity acting on large $k_{\perp}$, μ_m is the hyperviscosity acting on lare $k_{\parallel}$ and α is the large-scale friction coefficient. Finally, there is the parameter λ defined in equation (2.5). In the present framework, we are interested in monitoring the amplitude of the inverse cascade as a function of the parameter λ in the limit of large $Re_{\nu}, Re_{\mu}, Re_{\alpha}$ and large Λ.

Before we describe the simulations performed for this work, we define a few quantities of interest which we will use in the following. The 2-D energy spectrum is defined as

$$E(k_{\perp}, k_{\parallel}) = \frac{1}{2} \sum_{\substack{\mathbf{p}_{\perp} \\ k_{\perp} - \frac{1}{2} \leqslant p_{\perp} < k_{\perp} + \frac{1}{2}}} \left(\frac{|\hat{\omega}_{\parallel}(\mathbf{p}_{\perp}, k_{\parallel})|^2}{p_{\perp}^2} + |\hat{u}_{\parallel}(\mathbf{p}_{\perp}, k_{\parallel})|^2 \right), \tag{3.3}$$

where hats denote Fourier transforms. The 1-D energy spectrum is obtained from (3.3) by summation over $k_{\parallel}$,

$$E(k_{\perp}) = \sum_{k_{\parallel}} E(k_{\perp}, k_{\parallel}) \equiv E_{\perp}(k_{\perp}) + E_{\parallel}(k_{\perp}), \tag{3.4}$$

where $E_{\perp}$ contains all terms involving $\hat{\omega}_{\parallel}$ and $E_{\parallel}$ contains all terms involving $\hat{u}_{\parallel}$. The 2-D dissipation spectrum is defined as

$$D(k_{\perp}, k_{\parallel}) = \sum_{\substack{\mathbf{p}_{\perp} \\ k_{\perp} - \frac{1}{2} \leqslant p_{\perp} < k_{\perp} + \frac{1}{2}}} \left[\left(\nu_n p_{\perp}^{2n} + \mu_m k_{\parallel}^{2m} \right) \left(\frac{|\hat{\omega}_{\parallel}(\mathbf{p}_{\perp}, k_{\parallel})|^2}{p_{\perp}^2} + |\hat{u}_{\parallel}(\mathbf{p}_{\perp}, k_{\parallel})|^2 \right) \right]. \tag{3.5}$$

The large-scale energy dissipation rate is given by:

$$\epsilon_{\alpha} = \alpha \sum_{\mathbf{k}, |\mathbf{k}_{\perp}| \leqslant 2} |\hat{u}(\mathbf{k})|^2 \tag{3.6}$$

Set	A	B	C
Re_ν	3.1×10^3	4.9×10^5	4.9×10^5
Λ	32	32	64
resolution	$512^2 \times n_z$	$1024^2 \times n_z$	$1024^2 \times n_z$
# runs	16	9	9
# τ_{eddy}	22000	2500	7000

TABLE 1. Summary of the different simulations performed, where the resolution n_z in the parallel direction is varied between 128 and 512 in order to ensure well-resolved simulations. For each column, "# runs" different values of λ, as defined in (2.5), were investigated and $\#\tau_{eddy}$ gives the number of eddy turnover times $\tau_f = \epsilon_{in}^{-1/3}\ell^{2/3}$ simulated for each set of runs.

that measures the rate energy cascades inversely to the largest scales of the system. Finally, the spectral energy flux in the perpendicular direction through a cylinder of radius $k_\perp$ in Fourier space is defined as

$$\Pi(k_\perp) = \left\langle (\mathbf{u}_\perp)_{k_\perp}^{<} \cdot [(\mathbf{u}_\perp \cdot \nabla)\mathbf{u}_\perp] \right\rangle, \tag{3.7}$$

where $\mathbf{u} = (\mathbf{u}_\perp, \mathbf{u}_\parallel)$, $\mathbf{u}_\perp = \hat{e}_\parallel \times \nabla\psi$ and

$$(\mathbf{u}_\perp)_{k_\perp}^{<} = \sum_{\substack{\mathbf{p} \\ p_\perp < k_\perp}} \hat{\mathbf{u}}_\perp(\mathbf{p}) \exp(i\mathbf{p} \cdot \mathbf{x}). \tag{3.8}$$

The code used to solve equations (3.1, 3.2) is based on the Geophysical High-order Suite for Turbulence, using pseudo-spectral methods including 2/3 aliasing to solve for the flow in the triply periodic domain, (see Mininni *et al.* 2011). We performed three sets of experiments, one at resolution $512^2 \times n_z$ (set A) and two at $1024^2 \times n_z$ (sets B and C), where the resolution n_z in the parallel direction is varied depending on λ from 128 to 512 to ensure well-resolvedness at minimum computational cost. We choose either $\Lambda = 32$ (sets A and B) or $\Lambda = 64$ (set C). The parameters ν_n and μ_m are chosen for every simulation so that the run is well-resolved at large $k_\parallel, k_\perp$. This is checked by verifying that the maximum dissipation is captured within the interior of the 2-D dissipation spectrum (3.5). The coefficient α was chosen so that that the 1-D spectrum (3.4) does not have a maximum at $k = 1$ (i.e. no condensate is formed). In each of the three sets of experiments, we keep Λ and Re_ν fixed and vary λ from small (slow rotation) to large (fast rotation). A summary is given in table 1.

In all simulations, we monitor the 1-D and 2-D energy spectra (3.4, 3.3) as well as the large-scale dissipation rate (3.6). Simulations are continued until a steady state is reached where the large-scale dissipation rate and the energy spectrum are statistically steady, with the 1-D energy spectrum not having its maximum at $k = 1$. Note that in such a steady-state situation $\epsilon_{in} = \epsilon_\alpha + \epsilon_{\nu,\mu}$, where $\epsilon_{\nu,\mu} = \sum_{\mathbf{k}} D(k_\perp, k_\parallel)$ is the dissipation rate due to hyperviscosity in the parallel and perpendicular directions, dominantly occurring at small scales. Monitoring ϵ_α thus gives the amount of energy transferred inversely up to the largest scales $k = 1, 2$ and allows to measure the strength of the inverse cascade. Despite the fact that we solve asymptotically reduced equations, which allows larger time steps, the required simulation time was non-negligible, since convergence to the steady state was slow in some cases. In total, more than 30000 forcing-scale-based eddy turnover times $\tau_f = \epsilon^{-1/3}\ell^{2/3}$ were simulated, amounting to around two million CPU hours of computation time.

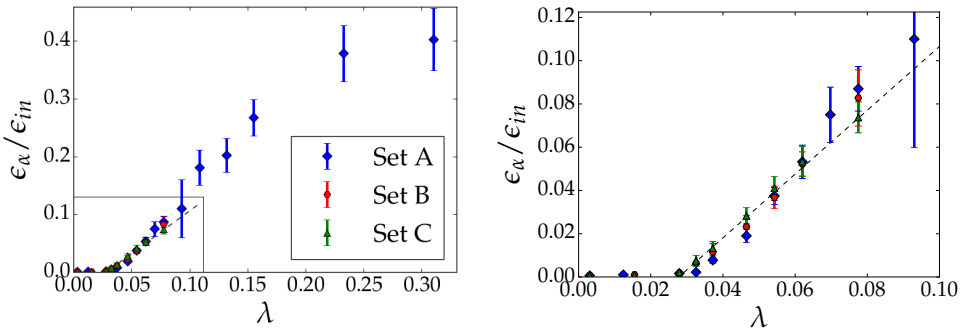

FIGURE 2. Large-scale dissipation rates as defined by (3.6) in steady state from sets A, B and C for different values of λ. Error bars correspond to standard deviation in steady state. The black dashed line is a linear fit based on set C. Right: all values of λ, Left: zoom close to $\lambda = \lambda_c$.

4. Results from direct numerical simulations

In this section, we present the results of the direct numerical simulations obtained in steady state. The central goal of this work is to determine the properties of the transition from a strictly forward cascade to a state that there is also an inverse cascade. The amplitude of the inverse cascade is given by the large-scale dissipation rate ϵ_α that measures the rate at which energy is transferred to the large scales. In the presence of an inverse cascade, ϵ_α converges to a finite value in the limit of $\Lambda, Re_\alpha, Re_\mu, Re_\nu \to \infty$ while it converges to zero in the absence of an inverse cascade. In Figure 2 we show ϵ_α (time averaged at steady-state) as a function of the parameter λ from all simulations. One observes a transition from $\epsilon_\alpha/\epsilon_{in} \approx 0$ to finite values at $\lambda = \lambda_c \approx 0.03$. At $\lambda < \lambda_c$ no inverse cascade is present and a vanishingly small amount energy reaches the scales $k_\perp = 1, 2$, where the large-scale dissipation acts. However, for $\lambda > \lambda_c$ an inverse cascade develops, whose strength increases monotonically with $\lambda - \lambda_c$, leading to non-zero large-scale dissipation. Comparing the curves obtained from sets A, B (Re_ν increased) and C (Re_ν and horizontal box size Λ increased), one observes that the transition appears to become sharper with increasing Reynolds number and box size, and remains at the same point. This indicates that the transition is likely to be critical and continuous, having a discontinuous 1st derivative at λ_c in the limit $Re_\nu, \Lambda \to \infty$. Considering only the highest Re_ν and Λ, i.e. set C only, we estimate from figure 2 that $\epsilon_\alpha \propto (\lambda - \lambda_c)^\gamma$ with $\gamma \approx 1$ from a fit close to onset, within our uncertainties. However, this estimate of the critical exponent is not definitive and a larger number of simulations and parameter values are needed to ascertain its precise value with higher confidence.

The left panel of figure 3 shows the energy flux in steady state for four values of λ from set A, namely (a) $\lambda = 0.0031$, (b) $\lambda = 0.00279$, (c) $\lambda = 0.062$ and (d) $\lambda = 0.155$. Cases (a) and (b) correspond to $\lambda < \lambda_c$, while for cases (c) and (d) $\lambda > \lambda_c$. All simulations present a significant forward energy flux for $k > k_f$. For $k \ll k_f$ the energy flux vanishes for the small-λ cases (a) & (b) (small rotation rates, tall boxes). Some inverse flux is observed for these cases, which is however confined to around $k \approx k_f/2$. By contrast, a non-vanishing inverse energy flux extending up to $k_\perp = 1$ is observed for the larger λ cases (c) & (d) (higher rotation rate, shallower box) that display an inverse cascade.

The right panel of 3 shows the corresponding 1-D spectra for the same four values of λ as in the left panel of the same figure. In cases (c) and (d), that display an inverse cascade, the spectrum is maximum at small wave numbers $k_\perp \simeq 2$. The reason why the spectrum does not peak at the smallest wavenumber $k = 1$ is the damping by the

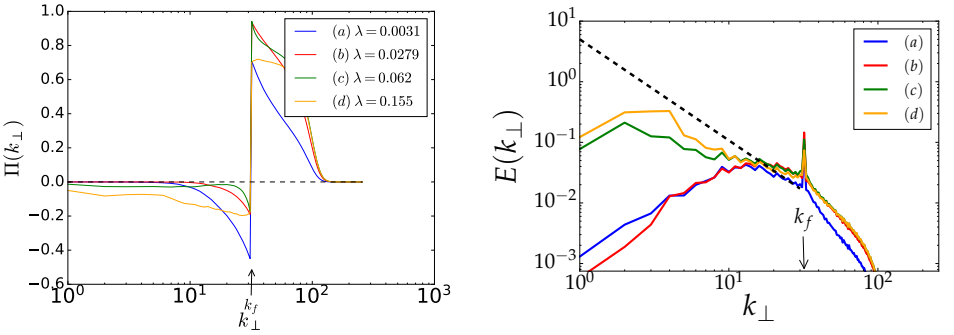

FIGURE 3. Energy flux in the perpendicular direction as a function of perpendicular wavenumber for four different values of λ from set A.

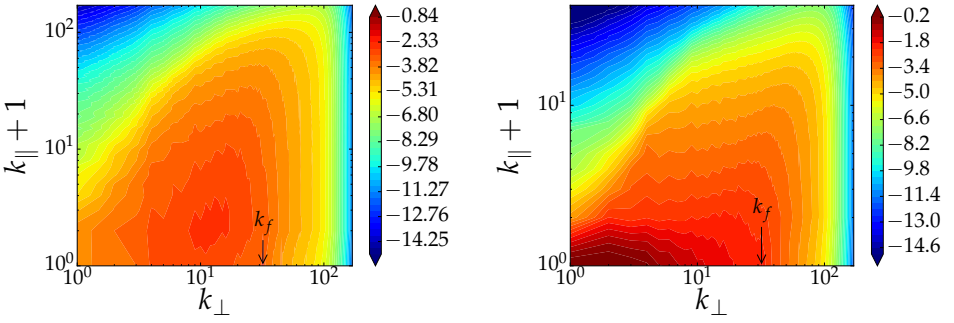

FIGURE 4. Steady-state 2-D energy spectra as defined in (3.3) from set A for $\lambda = 0.0279$ (left) and $\lambda = 0.155$ (right). Color bar logarithmic with base 10.

large-scale friction. In cases (a) and (b), the spectrum has two local maxima, one at the forcing scale $k_\perp = k_f$ and another one near $k_\perp = k_f/2$. This implies that there is transfer of energy to scales twice as large as the forcing scale. This, however, does not indicate an inverse cascade as this secondary peak remains close to the forcing scale and does not move further up to larger scales.

The 2-D spectra associated with cases (b) and (d) are presented in figure 4. They show that the secondary maximum observed in the 1-D energy spectra at $k_\perp \approx k_f/2$ for (b) stems from contributions at $k_\parallel > 0$. For $\lambda > \lambda_c$, the inverse energy cascade of the 2-D manifold leads to a maximum at $k_\parallel = 0$, at small $k_\perp$. Finally figure 5 shows the 1-D spectra from cases (b) and (d) decomposed to their horizontal $E_\perp(k_\perp)$ and parallel $E_\parallel(k_\perp)$ components. They show that perpendicular motions dominate for all wavenumbers $k < k_f$ in the case of an inverse cascade and also close to the secondary maximum at $k_f/2$ for the flows that do not display an inverse cascade. At large $k > k_f$ the two spectra are of the same order with $E_\parallel(k_\perp) > E_\perp(k_\perp)$.

The peak observed in the 1-D spectrum at $k \approx k_f/2$ is for the flows that do not display an inverse cascade is unexpected and deserves some further discussion. First we should note that this is not the first time a similar feature is observed. In Buzzicotti *et al.* (2018*b*), where simulations of rotating turbulence were performed, artificially excluding the $k_\parallel = 0$ plane in Fourier space showed a similar maximum. More recently such a maximum was also observed in simulations of rotating turbulence in elongated domains Clark Di Leoni *et al.* (2020). Since this is the statistically steady state of the system

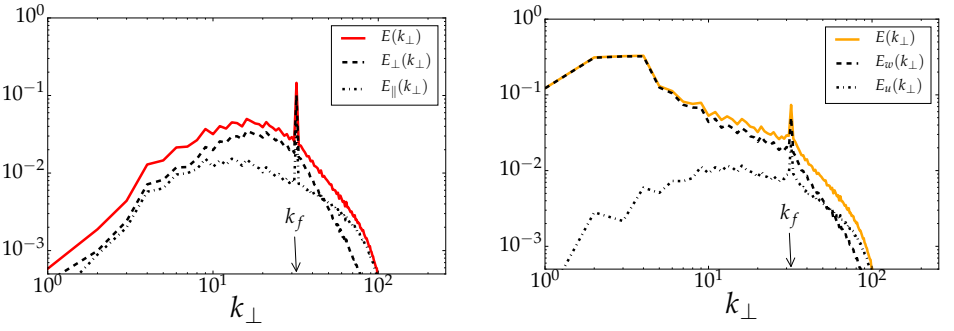

FIGURE 5. Left: Decomposition of spectrum at $\lambda = 0.0279$ into contributions $E_\perp$ from perpendicular motions and $E_\parallel$ from parallel motions. Right: same as left for $\lambda = 0.155$.

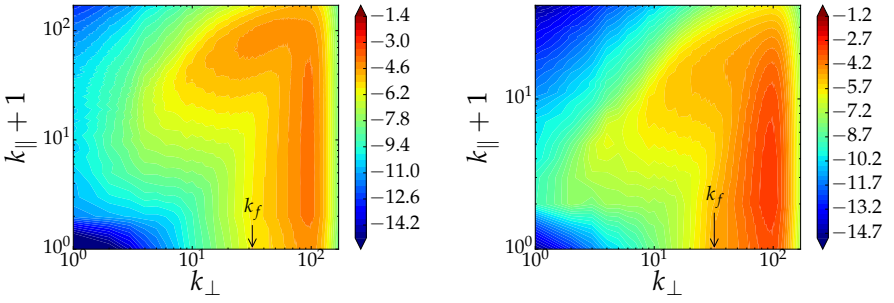

FIGURE 6. Steady-state 2-D dissipation spectra from set A for $\lambda = 0.0279$ (left) and $\lambda = 0.155$ (right). Color bar logarithmic with base 10.

and energy does not cascade further upscale, this inverse transfer does not stem from a turbulent inverse cascade, which would continue up to the largest scales, as it does for $\lambda < \lambda_c$. We have also verified that starting from initial conditions obtained from a run with $\lambda > \lambda_c$ and decreasing λ to a value below λ_c resulted, at long times, in a state with no inverse cascade. Rather, one may suspect an instability mechanism involving the forcing-scale flow. Indeed, considering a single homochiral wavenumber triad comprising one large-amplitude mode $\mathbf{k} = (k_f, 0, 0)$ at the forcing scale and the two small-amplitude modes at $\mathbf{p}, \mathbf{q}$, one finds that the modes with $q_\perp \approx k_f/2$, and $|q_\parallel| < k_f/\lambda$ are unstable (see appendix B). Interestingly, (Buzzicotti *et al.* 2018*b*) also found homochiral interactions to be responsible for the inverse energy transfer in their simulations. This instability can explain in part the transfer of energy to the $k_f/2$ modes. We note however that the maximum growth occurs at $q_\parallel = 0$ for the triad (see appendix B), which is not where the maximum is observed in the 2-D spectra shown in figure 4.

In figure 6 we also show the 2-D energy dissipation spectra for the same cases as in figure 4. The dissipation spectra demonstrate the well-resolvedness of the simulations: the maximum dissipation is within the simulation domain and not at the maximum wavenumbers (in the parallel or perpendicular direction). It is worth noting that most of the dissipation is occurring at large $k_\perp$ and not at large $k_\parallel$. The artificial hyper-viscosity used for the parallel wavenumbers in the simulations thus plays a minor role in dissipating energy. This is reassuring because in the asymptotic expansion (eqs. 2.6,2.7) only the perpendicular wavenumbers participate in the dissipation. It is also worth noting

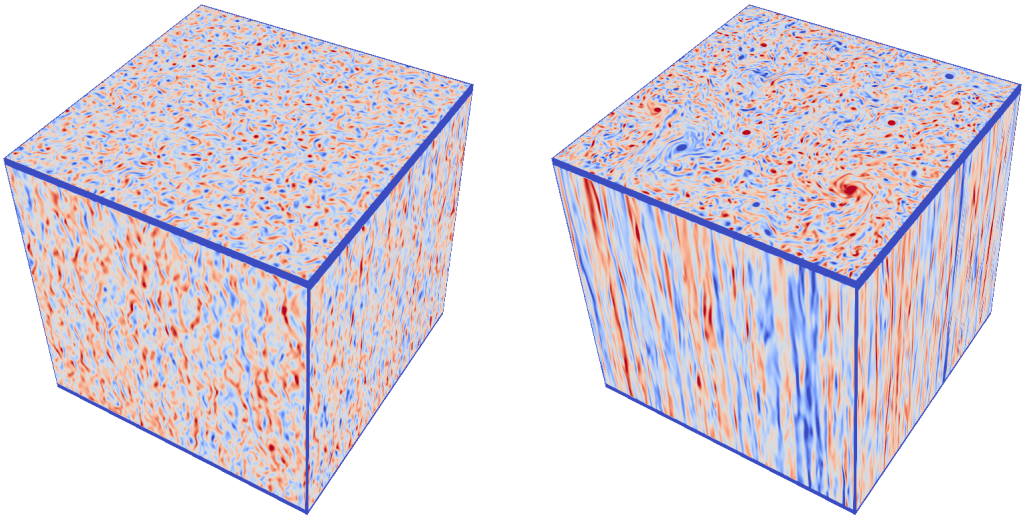

FIGURE 7. Visualisation of the flow in terms of vorticity $\omega_\parallel$ at $\lambda = 0.027 \lesssim \lambda_c$ (left) and $\lambda = 0.23 > \lambda_c$ (right). Positive vorticity in red, negative in blue, the edges have been coloured blue for better visualisation. For $\lambda > \lambda_c$, on the sides of the domain one can see elongated structures along the parallel direction, while the on top of the domain well-separated vortices are seen. For $\lambda < \lambda_c$, these elongated structures are absent. Furthermore, the flow for $\lambda > \lambda_c$ is characterised by larger perpendicular scales than the flow at $\lambda < \lambda_c$.

that for case (*b*) ($\lambda = 0.0279$) a higher resolution in the parallel direction was required than for case (d) ($\lambda = 0.155$). This is because the small-λ flows are more efficient at generating small scales in the parallel direction, while such generation is suppressed in large-λ flows by rotation.

Finally, figure 7 shows a visualisation of the flow in terms of vorticity $\omega_\parallel$ at $\lambda = 0.027 \lesssim \lambda_c$ (left) and $\lambda = 0.23 > \lambda_c$ (right). For $\lambda > \lambda_c$, columnar vortices are clearly visible which are approximately invariant along the axis of rotation. In the perpendicular direction these vortices are visibly of larger scale and organised in clusters. For $\lambda < \lambda_c$, no such anisotropic organisation of the flow can be observed.

5. Conclusions

The results presented in the sections above indicate that in fast-rotating turbulence within elongated domains, the transition from a strictly forward cascade to a split cascade (where part of the energy cascades inversely) is controlled by the parameter λ given in (2.5). This result implies that if the limit of infinite domain height $h \to \infty$ is taken for fixed Ro, then $\lambda \to 0$ and energy cascades forward as weak turbulence theory predicts. On the other hand, if the limit $Ro \to 0$ is taken for a fixed domain height, then $\lambda \to \infty$ and an inverse cascade will be present. The fact that a transition to an inverse cascade is observed in the asymptotic limit $h \propto \mathrm{Ro}^{-1} \to \infty$, which is considered here numerically, confirms the theoretical arguments presented in section 2. The phase space of rotating turbulence in the $(h, 1/Ro)$ plane, based on the present results is as depicted in figure 8. In the limit of infinite Re and Λ two phases exist, one where there is only forward cascade and one where there is a split cascade. They are separated by a critical line $h_c(Ro)$ that approaches the non-rotating critical height h_c^* for $\mathrm{Ro} \to \infty$, while for small Ro, which is the limit examined in the present work, h_c scales like $h_c = 1/(Ro\lambda_c)$ with $\lambda_c \simeq 0.03$.

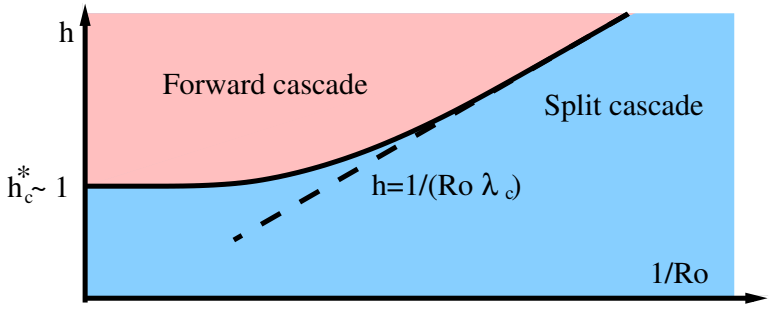

FIGURE 8. Phase space of rotating turbulence.

Our approach was based on asymptotic reduction, allowing us to reliably achieve the extreme parameter regimes required to test the theoretical predictions at comparatively moderate numerical cost. We stress, however, that a question of order of limit arises. By solving the asymptotically reduced equations and investigating increasing Re_ν and Λ in that framework, we are taking limits in the order

$$\lim_{\substack{Re_\nu\to\infty \\ \Lambda\to\infty}} \left(\lim_{\substack{\mathrm{Ro}\to 0 \\ \lambda=cst.}} \epsilon_\alpha(\lambda) \right) \quad \text{as opposed to} \quad \lim_{\substack{\mathrm{Ro}\to 0 \\ \lambda=cst.}} \left(\lim_{\substack{Re_\nu\to\infty \\ \Lambda\to\infty}} \epsilon_\alpha(\lambda) \right) \tag{5.1}$$

i.e. first the low Rossby limit (with fixed λ) is taken and then the large Reynolds number limit and not vice versa, which would correspond to studying the (Ro, H) dependence of an already fully turbulent flow. A priori, the two limits do not necessarily commute and therefore it is important to additionally study turbulent flow within an elongated domain in the full rotating Navier-Stokes system and to compare with the results obtained here.

Our numerical evidence also suggests that this transition is continuous but not smooth. The inverse cascade starts at a critical value λ_c with an almost linear dependence on the deviation from criticality $\epsilon_\alpha \propto (\lambda - \lambda_c)$. Despite the simplicity of this behaviour, its origin is far from being understood. Similar scaling behavior has been found for the transition to the inverse energy cascade in thin-layer turbulence below a critical layer height H_c (Benavides & Alexakis 2017) and for the two-dimensional magnetohydrodynamic flow studied in (Seshasayanan & Alexakis 2016; Seshasayanan *et al.* 2014). In both cases, a critical exponent close to unity is identified for the inverse energy transfer rate close to the transition. Future research should aim to provide an understanding of the origin of this estimated critical exponent. It should also verify which other turbulent fluid flows present criticality at the transition to the inversely cascading regime and whether their critical exponent is identical to or different from unity. Experimental investigations in such systems, where long-time averages can be performed, may prove invaluable in understanding this non-equilibrium phase transition.

Acknowledgements

This work was granted access to the HPC resources of MesoPSL financed by the Région Ile de France and the project Equip@Meso (reference ANR-10-EQPX-29-01) of the programme Investissements d'Avenir supervised by the Agence Nationale pour la Recherche and the HPC resources of GENCI-TGCC-CURIE & CINES Occigen (Project No. A0050506421 & A0070506421) where the present numerical simulations were performed. This work was also supported by the Agence nationale de la recherche (ANR DYSTURB project No. ANR-17-CE30-0004).

Declaration of interests

The authors report no conflict of interest.

Appendix A. Heuristic derivation of the fast-rotating long box equations

In this appendix we present a heuristic derivation of the reduced equations discussed in the main text. A derivation based on the method of multiple scales is given in (Sprague *et al.* 2006) for the Boussinesq equations, which reduces to our problem for vanishing density variations. The Navier-Stokes equation for a constant-density fluid in a system rotating at the constant rate $\boldsymbol{\Omega} = \Omega\hat{e}_\parallel$ is

$$\partial_t \mathbf{u} + \mathbf{u}\cdot\nabla\mathbf{u} + 2\Omega\hat{e}_\parallel \times \mathbf{u} = -\nabla p + \nu\nabla^2\mathbf{u} + \mathbf{f} \tag{A 1}$$

$$\nabla\cdot\mathbf{u} = 0, \tag{A 2}$$

where $\mathbf{u} = \mathbf{u}_\parallel + \mathbf{u}_\perp$ is velocity with $\mathbf{u}_\parallel = (\mathbf{u}\cdot\hat{e}_\parallel)\hat{e}_\parallel = u_\parallel\hat{e}_\parallel$ (we will use the same notation for all vectors), p is pressure (divided by the constant density ρ_0) and $\mathbf{f}$ is the forcing. We impose triply periodic boundary conditions, the forcing is assumed to be solenoidal and to have zero average over the domain.

Eliminating pressure from (A 1) using the incompressible projection defined for an arbitrary vector field $\mathbf{F}$ as $\mathbb{P}[\mathbf{F}] \equiv -\nabla^{-2}\nabla\times\nabla\times\mathbf{F} = \mathbf{F} - \nabla^{-2}\nabla(\nabla\cdot\mathbf{F})$, $\nabla^2(\nabla^{-2}f) = f$, and considering the equations for parallel velocity $u_\parallel$ and parallel vorticity $\omega_\parallel = \boldsymbol{\omega}\cdot\hat{e}_\parallel$, $\boldsymbol{\omega} = \nabla\times\mathbf{u}$, gives

$$\partial_t u_\parallel + \mathbf{u}\cdot\nabla u_\parallel \quad -\nabla^{-2}\nabla_\parallel\{\nabla\cdot(\mathbf{u}\cdot\nabla\mathbf{u})\} + 2\Omega\nabla^{-2}(\hat{e}_\parallel\cdot\nabla)\omega_\parallel = \nu\nabla^2 u_\parallel + f_\parallel \tag{A 3}$$

$$\partial_t\omega_\parallel + \mathbf{u}\cdot\nabla\omega_\parallel \quad -(2\Omega\hat{e}_\parallel + \boldsymbol{\omega})\cdot\nabla u_\parallel = \nu\nabla^2\omega_\parallel + f_\omega, \tag{A 4}$$

where $f_\omega \equiv \hat{e}_\parallel\cdot(\nabla\times\mathbf{f})$. We consider the limit of simultaneously fast rotation rates and large aspect ratios, $\Omega = \hat{\Omega}/\epsilon$ and $\mathbf{x} = \mathbf{x}_\perp + \hat{\mathbf{x}}_\parallel/\epsilon$, where $\epsilon \ll 1$ and all $\hat{\Omega}, x_\perp, \hat{x}_\parallel$ are all order one (omit hats from now on). The coordinate transformation implies $\nabla = \nabla_\perp + \epsilon\nabla_\parallel$, such that $\nabla^2 = \nabla_\perp^2 + O(\epsilon)$ and also $\nabla^{-2} = \nabla_\perp^{-2} + O(\epsilon)$. Importantly, in this limit the Coriolis terms in equations (A 3) and (A 4) are of order one since the largeness of the rotation rate Ω/ϵ and the smallness of parallel derivatives $\epsilon\nabla_\parallel$ compensate each other. The fact that only slow variations along the rotation axis are permitted derives from the Taylor-Proudman theorem forbidding fast variations in the limit $\mathrm{Ro}\to 0$.

Unlike in conventional quasi-geostrophy (in a thin layer), both perpendicular and parallel velocities, as well as their perpendicular derivatives, are assumed to be of order one. An important simplification arises from continuity,

$$\nabla\cdot\mathbf{u} = \nabla_\perp\cdot\mathbf{u}_\perp + O(\epsilon) = 0. \tag{A 5}$$

This means that the leading-order perpendicular velocity is incompressible and admits a streamfunction: $\mathbf{u}_\perp = \hat{e}_\parallel\times\nabla_\perp\psi$, hence $\omega_\parallel = \nabla_\perp^2\psi$. Another simplification arises from the fact that

$$\nabla^{-2}(\hat{e}_\parallel\cdot\nabla)\{\nabla\cdot(\mathbf{u}\cdot\nabla\mathbf{u})\} = O(\epsilon) \ll \mathbf{u}\cdot\nabla u_\parallel = \mathbf{u}_\perp\cdot\nabla_\perp u_\parallel + O(\epsilon). \tag{A 6}$$

Finally, one finds that the vortex stretching term in the parallel vorticity equation vanishes to at leading order $\boldsymbol{\omega}\cdot\nabla u_\parallel = O(\epsilon)$. The above results yield the leading-order governing equations

$$\partial_t u_\parallel + \mathbf{u}_\perp\cdot\nabla_\perp u_\parallel \quad +\nabla_\perp^{-2}(2\boldsymbol{\Omega}\cdot\nabla)\omega_\perp = \nu\nabla_\perp^2 u_\parallel + f_\parallel, \tag{A 7}$$

$$\partial_t\omega_\parallel + \mathbf{u}_\perp\cdot\nabla_\perp\omega_\parallel \quad -(2\boldsymbol{\Omega}\cdot\nabla)u_\parallel = \nu\nabla_\perp^2\omega_\parallel + f_\omega. \tag{A 8}$$

Equations (A 7, A 8) are complemented by the geostrophic balance relation in the perpendicular direction, $\mathbf{u}_\perp = \hat{e}_\parallel \times \nabla_\perp \psi$, which implies $\omega_\parallel = \nabla_\perp^2 \psi$, making (A 7, A 8) two equations for the two unknowns $u_\parallel$ and $\omega_\parallel$.

Appendix B. Homochiral triad instability

For concreteness, choose $\hat{e}_\parallel = \hat{e}_z$. The Fourier transformed governing equations (2.7,2.6) then read, in the absence of forcing or dissipation,

$$\partial_t \hat{u}_k - 2i\Omega \frac{k_\parallel}{k_\perp^2} \hat{\omega}_k = - \sum_{\mathbf{p}+\mathbf{q}+\mathbf{k}=0} [p_x q_y - q_x p_y] \frac{\hat{\omega}_p^*}{p_\perp^2} \hat{u}_q^*, \tag{B 1}$$

$$\partial_t \hat{\omega}_k - 2i\Omega k_z \hat{u}_k = - \sum_{\mathbf{p}+\mathbf{q}+\mathbf{k}=0} [p_x q_y - q_x p_y] \frac{\hat{\omega}_p^*}{p_\perp^2} \hat{\omega}_q^*, \tag{B 2}$$

where we used $u_\parallel \equiv \sum_{\mathbf{k}} \hat{u}_k e^{-i\mathbf{k}\cdot\mathbf{x}} \equiv \sum_{\mathbf{k}} \hat{u}_k e^{-i\mathbf{k}\cdot\mathbf{x}}$ and similarly for $\omega_\parallel = \nabla_h^2 \psi$, while expressing $\mathbf{u}_\perp$ via ψ. Defining $Z_{\mathbf{k}}^{s_\mathbf{k}} = \hat{u}_\mathbf{k} + s_\mathbf{k} \frac{\hat{\omega}_\mathbf{k}}{k_\perp}$, (B 1, B 2) may be rewritten entirely in terms of $Z_{\mathbf{k}}^{s_\mathbf{k}}$.

We consider a not necessarily resonant triad ($\mathbf{k}$,$\mathbf{p}$,$\mathbf{q}$) with $\mathbf{k} = (k_f, 0, 0)$, such that $p_x = -k_f - q_x$, $p_y = -q_y$, $p_z = -q_z$, choosing the forcing-scale mode $Z_\mathbf{k}^+ = u_0$, $Z_\mathbf{k}^- = 0 \Leftrightarrow \hat{\mathbf{u}}_k = u_0(0, -i/2, 1/2)$, i.e. the positively helical flow $\mathbf{u} = u_0(0, \sin(k_f x), \cos(k_f x))$. We take the modes at $\mathbf{p}$ and $\mathbf{q}$ to be of small amplitude, and perform a linear stability analysis of this configuration for the homochiral case $s_\mathbf{p} = s_\mathbf{q} = 1 = s_\mathbf{k}$ (the other cases do not give relevant results). We thus determine the growth rate $\sigma(\mathbf{q})$ of the two small-amplitude modes ($\mathbf{p}$ is uniquely determined by $\mathbf{q}$).

The left panel of figure 9 shows that the maximum of σ occurs for $q_\perp \approx k_f/2$, which points to a possible explanation of the maximum in the 1-D energy spectra found in figure 5 at $\lambda < \lambda_c$. A more detailed analysis is required, however, since the right panel of figure 9 indicates that the maximum growth rate due to the triad instability is located at $q_\parallel = 0$, whereas the DNS showed a spectral maximum at non-zero parallel wavenumber.

An interesting property of the growth rate obtained for the homochiral triad instability is that it vanishes above a certain threshold value of $q_\parallel^* \propto (H\tilde{\lambda})^{-1}$, with $\tilde{\lambda} = (k_f H)^{-1}(u_0 k_f/\Omega)^{-1}$ being the analogue, in the linear stability problem, of λ defined in eq. (2.5) for forced turbulence. For a given finite layer height $2\pi H$, there is a minimum $q_\parallel^{min} H = 1$ by periodic boundary conditions. At small $\tilde{\lambda}$, $q_\parallel^{min}$ will lie inside the range of unstable wavenumbers and thus the triad stability can occur. Increasing $\tilde{\lambda}$ (e.g. by decreasing H), a point is reached where $q_\parallel^{min}$ ceases to be unstable to the triad instability. This happens at $\tilde{\lambda} = \tilde{\lambda}_c \approx 0.35$. This point is related to the critical transition studied in the present paper, since when the triad instability is absent, there is no more transfer from the large-amplitude 2-D mode to the 3-D modes. This is precisely the criterion we identified for the transition to occur. When decoupled form 3-D motions, the 2-D modes of the flow will transfer energy inversely. The fact that $\tilde{\lambda}_c$ is different from λ_c does not invalidate this, given the drastic reduction from the DNS to a single wavenumber triad.

REFERENCES

Alexakis, A. 2011 Two-dimensional behavior of three-dimensional magnetohydrodynamic flow with a strong guiding field. *Phys. Rev. E* **84** (5), 056330.

Alexakis, A. 2015 Rotating taylor–green flow. *J. Fluid Mech.* **769**, 46–78.

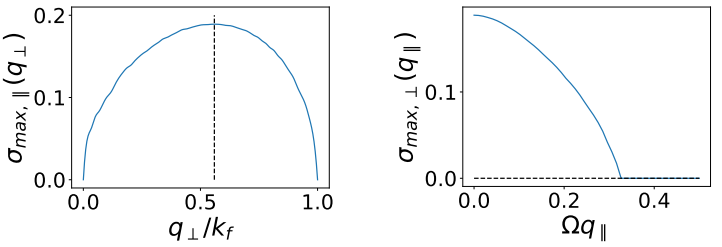

FIGURE 9. Left: Maximum (maximised over $q_\parallel$) growth rate as a function of $q_\perp$. The maximum is found for $q_\perp \approx k_f/2$. Right: Maximum (maximised over $q_\perp$) growth rate as a function of $\Omega q_\parallel$ with $k_f = 1$. There is a monotonic decay with $q_\parallel$.

ALEXAKIS, ALEXANDROS & BIFERALE, LUCA 2018 Cascades and transitions in turbulent flows. *Physics Reports* **767**, 1–101.

BAROUD, CHARLES N, PLAPP, BRENDAN B, SHE, ZHEN-SU & SWINNEY, HARRY L 2002 Anomalous self-similarity in a turbulent rapidly rotating fluid. *Physical Review Letters* **88** (11), 114501.

BAROUD, CHARLES N, PLAPP, BRENDAN B, SWINNEY, HARRY L & SHE, ZHEN-SU 2003 Scaling in three-dimensional and quasi-two-dimensional rotating turbulent flows. *Physics of Fluids* **15** (8), 2091–2104.

BARTELLO, P., MÉTAIS, O. & LESIEUR, M. 1994 Coherent structures in rotating three-dimensional turbulence. *J. Fluid Mech.* **273**, 1–29.

BENAVIDES, S. J. & ALEXAKIS, A. 2017 Critical transitions in thin layer turbulence. *J. Fluid Mech.* **822**, 364–385.

BIFERALE, LUCA, BONACCORSO, FABIO, MAZZITELLI, IRENE M, VAN HINSBERG, MICHEL AT, LANOTTE, ALESSANDRA S, MUSACCHIO, STEFANO, PERLEKAR, PRASAD & TOSCHI, FEDERICO 2016 Coherent structures and extreme events in rotating multiphase turbulent flows. *Physical Review X* **6** (4), 041036.

BOFFETTA, G. & ECKE, R. E. 2012 Two-dimensional turbulence. *Ann. Rev. Fluid Mech.* **44** (1), 427–451.

BUZZICOTTI, MICHELE, ALUIE, HUSSEIN, BIFERALE, LUCA & LINKMANN, MORITZ 2018*a* Energy transfer in turbulence under rotation. *Physical Review Fluids* **3** (3), 034802.

BUZZICOTTI, MICHELE, DI LEONI, PATRICIO CLARK & BIFERALE, LUCA 2018*b* On the inverse energy transfer in rotating turbulence. *The European Physical Journal E* **41** (11), 131.

CALKINS, MICHAEL A, JULIEN, KEITH, TOBIAS, STEVEN M & AURNOU, JONATHAN M 2015 A multiscale dynamo model driven by quasi-geostrophic convection. *Journal of Fluid Mechanics* **780**, 143–166.

CAMPAGNE, ANTOINE, GALLET, BASILE, MOISY, FRÉDÉRIC & CORTET, PIERRE-PHILIPPE 2014 Direct and inverse energy cascades in a forced rotating turbulence experiment. *Physics of Fluids* **26** (12), 125112.

CAMPAGNE, ANTOINE, GALLET, BASILE, MOISY, FRÉDÉRIC & CORTET, PIERRE-PHILIPPE 2015 Disentangling inertial waves from eddy turbulence in a forced rotating-turbulence experiment. *Physical Review E* **91** (4), 043016.

CAMPAGNE, ANTOINE, MACHICOANE, NATHANAËL, GALLET, BASILE, CORTET, PIERRE-PHILIPPE & MOISY, FRÉDÉRIC 2016 Turbulent drag in a rotating frame. *Journal of Fluid Mechanics* **794**.

CELANI, A., MUSACCHIO, S. & VINCENZI, D. 2010 Turbulence in more than two and less than three dimensions. *Phys. Rev. Lett.* **104**, 184506.

CHANTRY, MATTHEW, TUCKERMAN, LAURETTE S & BARKLEY, DWIGHT 2017 Universal continuous transition to turbulence in a planar shear flow. *Journal of Fluid Mechanics* **824**.

CHEN, QIAONING, CHEN, SHIYI, EYINK, GREGORY L & HOLM, DARRYL D 2005 Resonant interactions in rotating homogeneous three-dimensional turbulence. *Journal of Fluid Mechanics* **542**, 139–164.

Clark Di Leoni, Patricio, Buzzicotti, Michele, Alexakis, Alexandros & Biferale, Luca 2020 Energy transfer in turbulence under rotation. *to appear* .

Deusebio, E., Boffetta, G., Lindborg, E. & Musacchio, S. 2014 Dimensional transition in rotating turbulence. *Phys. Rev. E* **90** (2), 023005.

Dickinson, Stuart C & Long, Robert R 1983 Oscillating-grid turbulence including effects of rotation. *Journal of Fluid Mechanics* **126**, 315–333.

Duran-Matute, Matias, Flór, Jan-Bert, Godeferd, Fabien S & Jause-Labert, Clément 2013 Turbulence and columnar vortex formation through inertial-wave focusing. *Physical Review E* **87** (4), 041001.

Favier, Benjamin, Godeferd, FS & Cambon, Claude 2010 On space and time correlations of isotropic and rotating turbulence. *Physics of Fluids* **22** (1), 015101.

Frisch, U. 1995 *Turbulence: the legacy of AN Kolmogorov*. Cambridge University Press.

Gallet, Basile 2015 Exact two-dimensionalization of rapidly rotating large-reynolds-number flows. *Journal of Fluid Mechanics* **783**, 412–447.

Galtier, Sébastien 2003 Weak inertial-wave turbulence theory. *Physical Review E* **68** (1), 015301.

Godeferd, FS & Lollini, L 1999 Direct numerical simulations of turbulence with confinement and rotation. *Journal of Fluid Mechanics* **393**, 257–308.

Goldenfeld, Nigel & Shih, Hong-Yan 2017 Turbulence as a problem in non-equilibrium statistical mechanics. *Journal of Statistical Physics* **167** (3), 575–594.

Greenspan, Harvey Philip Greenspan & others 1968 *The theory of rotating fluids*. CUP Archive.

Grooms, Ian, Julien, Keith, Weiss, Jeffrey B & Knobloch, Edgar 2010 Model of convective taylor columns in rotating rayleigh-bénard convection. *Physical review letters* **104** (22), 224501.

Hopfinger, EJ, Browand, FK & Gagne, Y 1982 Turbulence and waves in a rotating tank. *Journal of Fluid Mechanics* **125**, 505–534.

Hough, Sydney Samuel 1897 Ix. on the application of harmonic analysis to the dynamical theory of the tides.—part i. on laplace's "oscillations of the first species" and the dynamics of ocean currents. *Philosophical Transactions of the Royal Society of London. Series A, Containing Papers of a Mathematical or Physical Character* (189), 201–257.

Ibbetson, A & Tritton, DJ 1975 Experiments on turbulence in a rotating fluid. *Journal of Fluid Mechanics* **68** (4), 639–672.

Julien, Keith, Knobloch, Edgar, Milliff, Ralph & Werne, Joseph 2006 Generalized quasi-geostrophy for spatially anisotropic rotationally constrained flows. *Journal of Fluid Mechanics* **555**, 233–274.

Julien, Keith, Knobloch, Edgar, Rubio, Antonio M & Vasil, Geoffrey M 2012*a* Heat transport in low-rossby-number rayleigh-bénard convection. *Physical review letters* **109** (25), 254503.

Julien, Keith, Knobloch, Edgar & Werne, Joseph 1998 A new class of equations for rotationally constrained flows. *Theoretical and computational fluid dynamics* **11** (3-4), 251–261.

Julien, K, Rubio, AM, Grooms, I & Knobloch, E 2012*b* Statistical and physical balances in low rossby number rayleigh–bénard convection. *Geophysical & Astrophysical Fluid Dynamics* **106** (4-5), 392–428.

van Kan, Adrian & Alexakis, Alexandros 2019 Condensates in thin-layer turbulence. *Journal of Fluid Mechanics* **864**, 490–518.

van Kan, Adrian, Nemoto, Takahiro & Alexakis, Alexandros 2019 Rare transitions to thin-layer turbulent condensates. *Journal of Fluid Mechanics* **878**, 356–369.

Lemoult, Grégoire, Shi, Liang, Avila, Kerstin, Jalikop, Shreyas V, Avila, Marc & Hof, Björn 2016 Directed percolation phase transition to sustained turbulence in couette flow. *Nature Physics* **12** (3), 254.

Machicoane, Nathanaël, Moisy, Frédéric & Cortet, Pierre-Philippe 2016 Two-dimensionalization of the flow driven by a slowly rotating impeller in a rapidly rotating fluid. *Physical Review Fluids* **1** (7), 073701.

Manneville, Paul 2009 Spatiotemporal perspective on the decay of turbulence in wall-bounded flows. *Physical Review E* **79** (2), 025301.

Marino, Raffaele, Mininni, Pablo Daniel, Rosenberg, Duane & Pouquet, Annick 2013 Inverse cascades in rotating stratified turbulence: fast growth of large scales. *EPL (Europhysics Letters)* **102** (4), 44006.

Marino, R., Pouquet, A. & Rosenberg, D. 2015 Resolving the paradox of oceanic large-scale balance and small-scale mixing. *Phys. Rev. Lett.* **114** (11), 114504.

Mininni, Pablo D, Alexakis, Alexandros & Pouquet, Annick 2009 Scale interactions and scaling laws in rotating flows at moderate rossby numbers and large reynolds numbers. *Physics of Fluids* **21** (1), 015108.

Mininni, Pablo Daniel & Pouquet, Annick 2010 Rotating helical turbulence. i. global evolution and spectral behavior. *Physics of Fluids* **22** (3), 035105.

Mininni, P. D., Rosenberg, D., Reddy, R. & Pouquet, A. 2011 A hybrid mpi–openmp scheme for scalable parallel pseudospectral computations for fluid turbulence. *Parallel Computing* **37** (6-7), 316–326.

Morize, C & Moisy, F 2006 Energy decay of rotating turbulence with confinement effects. *Physics of Fluids* **18** (6), 065107.

Moxey, David & Barkley, Dwight 2010 Distinct large-scale turbulent-laminar states in transitional pipe flow. *Proceedings of the National Academy of Sciences* **107** (18), 8091–8096.

Musacchio, S. & Boffetta, G. 2017 Split energy cascade in turbulent thin fluid layers. *Phys. Fluids* **29** (11), 111106.

Musacchio, Stefano & Boffetta, Guido 2019 Condensate in quasi-two-dimensional turbulence. *Physical Review Fluids* **4** (2), 022602.

Nazarenko, Sergei V & Schekochihin, Alexander A 2011 Critical balance in magnetohydrodynamic, rotating and stratified turbulence: towards a universal scaling conjecture. *Journal of Fluid Mechanics* **677**, 134–153.

Pedlosky, J. 2013 *Geophysical fluid dynamics*. Springer Science & Business Media.

Pestana, Tiago & Hickel, Stefan 2019 Regime transition in the energy cascade of rotating turbulence. *Physical Review E* **99** (5), 053103.

Pomeau, Yves 1986 Front motion, metastability and subcritical bifurcations in hydrodynamics. *Physica D: Nonlinear Phenomena* **23** (1-3), 3–11.

Pouquet, A, Rosenberg, D, Stawarz, JE & Marino, R 2019 Helicity dynamics, inverse, and bidirectional cascades in fluid and magnetohydrodynamic turbulence: a brief review. *Earth and Space Science* **6** (3), 351–369.

Proudman, Joseph 1916 On the motion of solids in a liquid possessing vorticity. *Proceedings of the Royal Society of London. Series A, Containing Papers of a Mathematical and Physical Character* **92** (642), 408–424.

Rubio, A. M., Julien, K., Knobloch, E. & Weiss, J. B. 2014 Upscale energy transfer in three-dimensional rapidly rotating turbulent convection. *Phys. Rev. Lett.* **112** (14), 144501.

Sahoo, G., Alexakis, A. & Biferale, L. 2017 Discontinuous transition from direct to inverse cascade in three-dimensional turbulence. *Phys. Rev. Lett.* **118** (16), 164501.

Sahoo, G. & Biferale, L. 2015 Disentangling the triadic interactions in navier-stokes equations. *Eur. Phys. J. E* **38** (10), 114.

Sen, Amrik, Mininni, Pablo D, Rosenberg, Duane & Pouquet, Annick 2012 Anisotropy and nonuniversality in scaling laws of the large-scale energy spectrum in rotating turbulence. *Physical Review E* **86** (3), 036319.

Seshasayanan, K. & Alexakis, A. 2016 Critical behavior in the inverse to forward energy transition in two-dimensional magnetohydrodynamic flow. *Phys. Rev. E* **93** (1), 013104.

Seshasayanan, K. & Alexakis, A. 2018 Condensates in rotating turbulent flows. *J. Fluid Mech.* **841**, 434–462.

Seshasayanan, K., Benavides, S. J. & Alexakis, A. 2014 On the edge of an inverse cascade. *Phys. Rev. E* **90** (5), 051003.

Smith, L. M., Chasnov, J. R. & Waleffe, F. 1996 Crossover from two-to three-dimensional turbulence. *Phys. Rev. Lett.* **77** (12), 2467.

Smith, Leslie M & Waleffe, Fabian 1999 Transfer of energy to two-dimensional large scales in forced, rotating three-dimensional turbulence. *Physics of fluids* **11** (6), 1608–1622.

Sozza, A., Boffetta, G., Muratore-Ginanneschi, P. & Musacchio, S. 2015 Dimensional

transition of energy cascades in stably stratified forced thin fluid layers. *Phys. Fluids* **27** (3), 035112.

Sprague, Michael, Julien, Keith, Knobloch, Edgar & Werne, Joseph 2006 Numerical simulation of an asymptotically reduced system for rotationally constrained convection. *Journal of Fluid Mechanics* **551**, 141–174.

Staplehurst, PJ, Davidson, PA & Dalziel, SB 2008 Structure formation in homogeneous freely decaying rotating turbulence. *Journal of Fluid Mechanics* **598**, 81–105.

Taylor, Geoffrey Ingram 1917 Motion of solids in fluids when the flow is not irrotational. *Proceedings of the Royal Society of London. Series A, Containing Papers of a Mathematical and Physical Character* **93** (648), 99–113.

Thiele, Mark & Müller, Wolf-Christian 2009 Structure and decay of rotating homogeneous turbulence. *Journal of Fluid Mechanics* **637**, 425–442.

Valente, Pedro C & Dallas, Vassilios 2017 Spectral imbalance in the inertial range dynamics of decaying rotating turbulence. *Physical Review E* **95** (2), 023114.

Van Bokhoven, LJA, Clercx, HJH, Van Heijst, GJF & Trieling, RR 2009 Experiments on rapidly rotating turbulent flows. *Physics of Fluids* **21** (9), 096601.

Waleffe, Fabian 1993 Inertial transfers in the helical decomposition. *Physics of Fluids A: Fluid Dynamics* **5** (3), 677–685.

Yarom, Ehud & Sharon, Eran 2014 Experimental observation of steady inertial wave turbulence in deep rotating flows. *Nature Physics* **10** (7), 510.

Yarom, Ehud, Vardi, Yuval & Sharon, Eran 2013 Experimental quantification of inverse energy cascade in deep rotating turbulence. *Physics of Fluids* **25** (8), 085105.

Yeung, PK & Zhou, Ye 1998 Numerical study of rotating turbulence with external forcing. *Physics of Fluids* **10** (11), 2895–2909.

Yokoyama, N. & Takaoka, M. 2017 Hysteretic transitions between quasi-two-dimensional flow and three-dimensional flow in forced rotating turbulence. *Phys. Rev. Fluids* **2** (9), 092602.